ON THE CALCULATION OF SUPERSONIC SEPARATING AND REATTACHING FLOWS

By John D. Murphy, Leroy L. Presley, and William C. Rose

NASA Ames Research Center

SUMMARY

A method is developed for solving the laminar and turbulent compressible boundary-layer equations for separating and reattaching flows. Results of this method are compared with experimental data for two laminar and three turbulent boundary-layer, shock-wave interactions. Several Navier-Stokes solutions were obtained for each of the laminar boundary-layer, shock-wave interactions considered. Comparison of these solutions indicates a first-order sensitivity in C_f to the computational mesh selected in *both* the viscous and inviscid portions of the flow.

Three turbulent boundary-layer, shock-wave interactions were considered, one unseparated interaction at $M = 3$ and two separated interactions at $M = 1.47$ and 3. Boundary-layer theory appeared to be adequate to describe the first two of these interacting flows. However, for the separated interaction at $M = 3$, boundary-layer theory failed.

Comparison of the present boundary-layer solutions with the Navier-Stokes solutions and with data for a given Mach number indicates that as long as $|v_e/u_e|$ is small, the boundary-layer approximation yields solutions whose accuracy is comparable to the Navier-Stokes solutions. A more general parameter might indicate boundary-layer theory to be valid if some function of Mach number times $|v_e/u_e|$ is small.

Since the present boundary-layer solution is an inverse method, that is, $C_f(x)$ is specified rather than $P(x)$, a criterion for selecting the correct C_f distribution is required. It was originally anticipated that this criterion would be supplied by coupling the boundary-layer solutions to a shock-capturing, finite-difference solution to the inviscid-flow equations. Although several modes of coupling have been attempted, only slight success has been obtained to date because the shock-capturing scheme imposes a relatively thick shock wave on the viscous flow, which in turn requires an almost discontinuous change in flow angle at the boundary-layer edge. The inconsistency of this behavior in the two solutions has thus far obstructed attempts to obtain meaningful coupled solutions. Therefore, a truncated Navier-Stokes system of equations was examined and it appears that this technique circumvents these difficulties.

INTRODUCTION

It is generally agreed that the problem of separating and reattaching flows is one of the more challenging and technologically relevant problems in

computational fluid mechanics. In recent years, the computational attack has taken place on two fronts - the engineering approach by way of boundary-layer theory and the pure numerical approach by way of the Navier-Stokes equations. Reasonably complete summations of the status of these two approaches up to about 1970 are contained in references 1 to 3. During the past two or three years, substantial additional progress has been made in the boundary-layer theory approach by Klineberg and Steger (ref. 4) and Carter (ref. 5), and in the Navier-Stokes equation approach as represented by references 6 through 11. The basic position taken by each of these schools of thought can be summarized as follows: the Navier-Stokes equations are undoubtedly the correct equations for describing the flow fields in question and, since we can solve them, why settle for an approximation? The boundary-layer contingent would concur with the above but they would add that the cost of Navier-Stokes solutions both now and in the foreseeable future is far too high to permit their use as design tools.

The present study examines these positions in some detail. In particular, we are concerned with establishing, at least qualitatively, the limits of applicability of the boundary-layer approximation for both laminar and turbulent separating and reattaching flows. Secondly, we are concerned with the development of an economical and reasonably accurate engineering calculation scheme for such flows.

SYMBOLS

C	Chapman-Rubesin constant
C_f	skin-friction coefficient, $C_f = \tau_w/(1/2)\rho_o u_o^2$
DC	difference coefficient multiplying quantities at x
DM	difference coefficient multiplying quantities at $x-\Delta x$
DP	difference coefficient multiplying quantities at $x+\Delta x$
E	Eckert number, $u_e^2/2H_e$
F	defined in equation (12)
f	dimensionless stream function
H	total enthalpy $h + (u^2/2)$
h	static enthalpy
ℓ	mixing length
M_o	initial Mach number

M	number of nodes in x direction
N	number of nodes in y direction
p	pressure
Pr	Prandtl number
Pr_T	turbulent Prandtl number
R	gas constant
r	body radius
S	entropy
T	temperature
U	defined in equation (12)
u	velocity component in x direction
v	velocity component in y direction
x	streamwise variable
y	cross stream variable
α	weighting factor in type dependent differencing
β	boundary-layer pressure gradient parameter = $\frac{2\xi}{u_e}\frac{du_e}{d\xi}$
γ	ratio of specific heats
Δ	difference in quantities
δ	boundary-layer thickness or stream angle
δ^*	displacement thickness
ε	residual error
ζ	y_n/y_ℓ
ρ	density
σ	defined in equation (18)
μ	viscosity or Mach angle ($\mu = \sin^{-1}(1/M)$)
τ	shear stress

ξ	transformed x variable
η	transformed y variable
$( )'$	differentiation with respect to η

Subscripts

e	evaluated at boundary-layer edge
f	evaluated at final conditions downstream of interaction
i	evaluated at ith x point
j	evaluated at jth y point
ℓ	lower boundary
o	evaluated on initial line
t	evaluated at stagnation conditions
u	upper boundary
w	evaluated at wall conditions

ANALYSIS

Viscous-Flow Calculations

The procedure used to solve the viscous-flow portion of the calculation is a generalized Galerkin method (refs. 12 and 13) applied to the boundary-layer equations. The equations considered are

$$\frac{\partial \rho u r^k}{\partial x} + \frac{\partial \rho v r^k}{\partial y} = 0 \tag{1}$$

$$\rho u \frac{\partial u}{\partial x} + \rho v \frac{\partial u}{\partial y} = - \frac{dP}{dx} + \frac{\partial}{\partial y}\left(\mu \frac{\partial u}{\partial y} + \rho\tau\right) \tag{2}$$

$$\rho u \frac{\partial H}{\partial x} + \rho v \frac{\partial H}{\partial y} = \frac{\partial}{\partial y}\left[\frac{\mu}{Pr} \frac{\partial H}{\partial y} + \frac{\mu}{2}\left(1 - \frac{1}{Pr}\right) \frac{\partial u^2}{\partial y}\right] + \frac{\partial}{\partial y}\left\{\rho\tau\left[\frac{1}{Pr_T} \frac{\partial H/\partial y}{\partial u/\partial y} + u\left(1 - \frac{1}{Pr_T}\right)\right]\right\} \tag{3}$$

$$P = \rho R T \tag{4}$$

$$\rho\tau = \rho \ell^2 \left|\frac{\partial u}{\partial y}\right| \frac{\partial u}{\partial y} \tag{5}$$

Only adiabatic flows with $Pr = Pr_T = 1$ are treated here; hence equation (3) is replaced by $h + (u^2/2) = \text{const}$. To suppress the streamwise growth of the boundary layer and to facilitate initialization, equations (1) and (2) are combined under the Levy-Lees-Dorodnitsyn transformation $(x,y) \rightarrow (\xi,\eta)$ where

$$\xi = \int_o^x \rho_o u_o \mu_o r^{2k} dx \quad , \quad \eta = \frac{\rho_o u_o r^k}{\sqrt{2\xi}} \int_o^y \frac{\rho}{\rho_o} dy$$

$$f = \frac{1}{\sqrt{2\xi}} \int_o^y \rho u \, dy \quad , \quad f' = \frac{u}{u_e}$$

which results in

$$(Cf'')' + ff'' + \beta\left(\frac{\rho_e}{\rho} - f'^2\right) + K_1 \rho\tau - 2\xi\left(f' \frac{\partial f'}{\partial \xi} - f'' \frac{\partial f}{\partial \xi}\right) = 0 \qquad (6)$$

where $K_1 = \sqrt{2\xi}/\mu_e r^k$ and the primes indicate differentiation with respect to η. The following analysis closely parallels that of Kendall and Bartlett (ref. 13). The present method extends that of reference 13 to treat separated flow and is restricted to calorically and thermally perfect gases.

y-dependent differencing—To apply the generalized Galerkin method, the approximations for the stream functions, velocity, and shear between adjacent nodes are chosen as

$$f_{j+1} = f_j + f'_j \Delta\eta + f''_j \frac{\Delta\eta^2}{2} + f'''_j \frac{\Delta\eta^3}{3} + f'''_{j+1} \frac{\Delta\eta^3}{24} \qquad (7)$$

$$f'_{j+1} = f'_j + f''_j \Delta\eta + f'''_j \frac{\Delta\eta^2}{3} + f'''_{j+1} \frac{\Delta\eta^2}{6} \qquad (8)$$

$$f''_{j+1} = f''_j + f'''_j \frac{\Delta\eta^2}{2} + f'''_{j+1} \frac{\Delta\eta^2}{2} \qquad (9)$$

These relations are obtained by a Taylor series expansion to terms including f^{IV} and substitution of $f_j^{IV} = (f'''_{j+1} - f'''_j)/\Delta\eta$. Equations (7) to (9) are substituted in equation (6) and the results integrated with respect to a unit square-wave weighting function from η_j to η_{j+1} to yield:

$$Cf''\Big|_{\eta_j}^{\eta_{j+1}} + ff'\Big|_{\eta_j}^{\eta_{j+1}} - \left[1 + \frac{2\beta}{2-E}\right]\sum_{k=1}^{4} f_j^k \, XPK + \frac{\beta}{2-E}\,\eta\Big|_{\eta_j}^{\eta_{j+1}} + K_1\bar{\rho}\tau\Big|_{\eta_j}^{\eta_{j+1}}$$

$$-2\xi \int_{\eta_j}^{\eta_{j+1}} f' \frac{\partial f'}{\partial \xi} d\eta + 2\xi \int_{\eta_j}^{\eta_{j+1}} f'' \frac{\partial f}{\partial \xi} d\eta = 0 \qquad (10)$$

where

$$\sum_{k=1}^{4} f_j^k XPK = f_j' XP1 + f_j'' XP2 + f_j''' XP3 + f_{j+1}''' XP4 = \int f'^2 d\eta$$

and

$$XP1 = \Delta\eta\left(f_j' + f_j'' \frac{\Delta\eta}{2} + f_j''' \frac{\Delta\eta^2}{8} + f_{j+1}''' \frac{\Delta\eta^2}{24}\right)$$

$$XP2 = \frac{\Delta\eta^2}{2}\left(f_j' + f_j'' \frac{2\Delta\eta}{3} + f_j''' \frac{11\Delta\eta^2}{60} + f_{j+1}''' \frac{\Delta\eta^2}{15}\right)$$

$$XP3 = \frac{\Delta\eta^3}{8}\left(f_j' + f_j'' \frac{11\Delta\eta}{15} + f_j''' \frac{66\Delta\eta^2}{315} + f_{j+1}''' \frac{5\Delta\eta^2}{63}\right)$$

$$XP4 = \frac{\Delta\eta^3}{24}\left(f_j' + f_j'' \frac{4\Delta\eta}{5} + f_j''' \frac{5\Delta\eta^2}{21} + f_{j+1}''' \frac{2\Delta\eta^2}{21}\right)$$

The two terms remaining to be integrated are discussed under x-Dependent Differencing. This procedure yields a consistent differencing method that is fourth-order accurate in η and equations (7) to (9) ensure that the stream function, velocity, and shear are defined everywhere (not only at nodal points) and are continuous everywhere. Equations (7) to (10) provide a sequence of $4(N-1)$ equations in $4N$ unknowns, where N is the number of nodes normal to the wall. Note that $3(N-1)$ of these equations are linear algebraic equations while $(N-1)$ equations are nonlinear ordinary differential equations. The remaining four equations are imposed as boundary conditions:

$$f = f' = 0 \quad \text{at} \quad \eta = 0$$

$$f' = 1, \quad f'' = 0 \quad \text{at} \quad \eta = \infty$$

The complete system is solved by use of a Newton-Raphson iteration scheme by differentiating with respect to f_j, f_{j+1}, . . ., f_j''', f_{j+1}''', and for separated flows β, to yield

$$J(f)\Delta f_j^k = -\varepsilon_j^k$$

where $J(f)$ is the $(4N \times 4N)$ Jacobian, ε is the residual error, and Δf_j^k is the incremental change in the solution parameters per iteration.

To speed up the iteration process, the equations are ordered so that the $3(N-1)$ linear algebraic equations plus the boundary condition $f'(0) = 0$ occupy the first $3N-2$ matrix rows. The matrix has the partitioned form (see ref. 14):

$$\begin{bmatrix} L_1 & L_2 \\ NL_1 & NL_2 \end{bmatrix} \begin{bmatrix} \Delta f_L \\ \Delta f_{NL} \end{bmatrix} = - \begin{bmatrix} \varepsilon_L \\ \varepsilon_{NL} \end{bmatrix}$$

The submatrix L_1 is a function of the nodal configuration only and can be inverted just once and used in all subsequent calculations. Formal manipulation and back substitution yield

$$\Delta f_{NL} = \left[NL_2 - NL_1 L_1^{-1} L_2\right]^{-1}\left[-\epsilon_{NL} + NL_1 L_1^{-1}\epsilon_L\right]$$

$$\Delta f_L = L_1^{-1}\left[-\epsilon_L - L_2 \Delta f_{NL}\right]$$

The matrix $\left[NL_2 - NL_1 L_1^{-1} L_2\right]$ must be inverted every iteration, but it is only of order (N+2).

x-dependent differencing—The streamwise differencing is carried out in a manner similar to that of reference 4. The term

$$-2\xi \int_{\eta_j}^{\eta_{j+1}} f' \frac{\partial f'}{\partial \xi}\, d\eta$$

is decomposed and integrated by parts as

$$-\int_{\eta_j}^{\eta_{j+1}} f'\left[DPf'_{i+1} + DCf'_i + DMf'_{i-1}\right]d\eta = -\left[DP \sum f^k_{i+1,j} XPK + DC \sum f^k_{i,j} XPK + DM \sum f^k_{i-1,j} XPK\right]$$

where, for attached flow,

$$DP = 0\ , \quad DC = 2/\ell n\ \xi_i/\xi_{i-1}\ , \quad DM = -DC$$

and for separated flow

$$DP = (1-\alpha)/\ell n\ \xi_{i+1}/\xi_i \quad ; \quad \alpha = 1 \quad \text{for} \quad f' > 0.01$$

$$DM = -(1+\alpha)/\ell n\ \xi_i/\xi_{i-1} \quad ; \quad \alpha = 100f' \ , \quad -0.01 \le f' \le 0.01$$

$$DC = -(DP + DM) \quad ; \quad \alpha = -1 \ , \quad f' < -0.01$$

This procedure incorporates backward differencing when the flow is in the mainstream direction, forward differencing when the flow is reversed, and a central difference on and near the zero velocity streamline. The remaining term is decomposed as above, integrated by parts, and expanded in Taylor series to yield:

$$2\xi\int_{\eta_j}^{\eta_{j+1}} f''\frac{\partial f}{\partial \xi}\,d\eta = DC\ f_i f_i'\Big|_{\eta_j}^{\eta_{j+1}} + DP\ f_{i+1} f_i'\Big|_{\eta_j}^{\eta_{j+1}} + DM\ f_{i-1} f_i'\Big|_{\eta_j}^{\eta_{j+1}} + DC\sum f_{i,j}^{k}\,XPK_i$$

$$+DP\sum f_{ij}^{k}\,XPK_{i+1} + DM\sum f_{ij}^{k}\,XPK_{i-1}$$

where, for attached flow, excluding the points of separation and reattachment yields

$$DC = 2/\ell n\ \xi_i/\xi_{i-1}\ ,\quad DP = 0\ ,\quad DM = -DC$$

and for separated flow,

$$DC = 0\ ,\quad DP = 2/\ell n\ \xi_{i+1}/\xi_{i-1}\ ,\quad DM = -DP$$

As shown, a straightforward marching routine is used in the attached flow while, for separated flow, the entire separation region must be relaxed simultaneously.

The present method requires no under relaxation and a typical well-separated flow with 20 η points and 10 ξ points can be relaxed to a maximum residual $0(10^{-4})$ in about 22 iterations compared to 800 for the method of reference 4 and 100 to 200 iterations for the method of reference 5. Although the present method may require more operations per iteration, it is at least competitive with other methods cited. The speed of the present method primarily results from the splined Taylor series used as approximating functions. First, they provide an effective fourth-order-accurate, finite-difference representation in the y direction which permits a relatively sparse nodal array to yield high accuracy and, second, the spline character enhances the stability markedly.

Inviscid-Flow Equations and Coupling Schemes

In this section, the technique used to solve for the inviscid flow field and to obtain the effects due to the boundary layer on that flow is described. A technique for obtaining fully coupled interactive solutions of the inviscid and viscous flows is being developed, but is not sufficiently advanced to discuss here. Rather, at this point, boundary-layer solutions for a pressure and skin-friction distribution, appropriate to the data of reference 13, have been obtained and then various schemes for matching this solution with the inviscid flow have been investigated. The inviscid flow is for supersonic flow between a shock-wave generator and some matching line given by the boundary-layer solution.

Inviscid-flow equations—The basic equation used in the inviscid flow-field analysis is similar to that of reference 15. The key features, however,

are described here for completeness. In a Cartesian coordinate system, the steady, inviscid, two-dimensional fluid dynamic equations (continuity, x and y momentum) are written in conservative form as

$$\tilde{U}_x + \tilde{F}_y = 0 \tag{11}$$

The three components of the vectors $\tilde{U}$ and $\tilde{F}$, which represent the conservative variables, are defined as

$$\tilde{U} = \begin{bmatrix} \rho u \\ kp+\rho u^2 \\ \rho uv \end{bmatrix}, \quad \tilde{F} = \begin{bmatrix} \rho v \\ \rho uv \\ kp+\rho v^2 \end{bmatrix} \tag{12}$$

where $k = (\gamma-1)/2\gamma$. The units of these equations were normalized by dividing both pressure and density by their respective stagnation conditions, while the velocities were divided by the maximum adiabatic velocity. With this normalization and the further restriction that the flow be adiabatic, the energy equation can be written:

$$\frac{p}{\rho} + u^2 + v^2 = 1 \tag{13}$$

To calculate two-dimensional flow between two nonparallel walls, in this case the shock-wave generator and the lower coupling boundary, it is most convenient to normalize the coordinate system so that the upper and lower boundaries become parallel. The transformed coordinates are

$$\left.\begin{aligned} x &= x \\ \xi &= y - \frac{y_\ell}{y_u - y_\ell} = y - \frac{y_\ell}{\zeta} \end{aligned}\right\} \tag{14}$$

where $y_u = y_u(x)$ and $y_\ell = y_\ell(x)$. Applying this transformation to equation (11) results in

$$U_x + F_\zeta = 0 \tag{15}$$

where $U = \zeta\tilde{U}$ and $F = \tilde{F} + \tilde{U}\left[y'_\ell(\xi-1) - y'_u\right]$. (In this section, the primes denote differentiation with respect to x.)

The above differential equation is integrated using MacCormack's second-order-accurate differencing scheme (see ref. 15). For flow-field points, that is, points on neither the upper nor lower boundary, the predictor and corrector equations are

$$\bar{U}_j^{n+1} = U_j^n - \left(\frac{\Delta x}{\Delta \xi}\right)\left(F_{j+1}^n - F_j^n\right) \quad \text{(predictor)} \tag{16}$$

Subscript j identifies particular points on a data line as follows: 1, lower body point; 2, 3, . . ., $N_{\xi-1}$, flow-field points; and N_ξ, upper body point. The data lines are identified by the superscripts n and n+1. The bars indicate a predicted value.

$$U_j^{n+1} = \frac{1}{2}\left[U_j^n + \overline{U_j^{n+1}} - \left(\frac{\Delta x}{\Delta \xi}\right)\left(\overline{F_j^{n+1}} - \overline{F_{j-1}^{n+1}}\right)\right] \quad \text{(corrector)} \tag{17}$$

The above equations are applied to the three vector components of U.

The step size in the x direction is found by determining the maximum slope of the characteristic surface, inclined at the local Mach angle μ relative to the local stream angle δ, for each point as follows:

$$\sigma_j^n(\pm) = \left|\tan(\pm\mu + \delta)_j^n\right| \tag{18}$$

where the $\pm$ denote positive and negative directions of the Mach angle from each point. The entire data line n is surveyed to determine $\left|\sigma_j^n(\pm)\right|_{max}$. Depending on the sign associated with the maximum slope, Δx is found from

$$\Delta x(+) = K\left[\frac{\xi_{j+1}^{n+1}\zeta^{n+1} - \xi_j^n\zeta^n - y_\ell^n + y_\ell^{n+1}}{\sigma_j^n(+)_{max}}\right] \tag{19}$$

or

$$\Delta x(-) = K\left[\frac{\xi_j^n\zeta^n - \xi_{j-1}^{n+1}\zeta^{n+1} - y_\ell^{n+1} + y_\ell^n}{\sigma_j^n(-)_{max}}\right] \tag{20}$$

where K is a constant that controls the step size. If $K = 1$, the CFL condition is satisfied identically.

Application of the finite-difference equations (16) and (17) yields predicted and corrected values of the three components of the conservative-variable vector U on the new data line. These must be decoded after the predictor step and corrector step in turn. This decoding into physical variables is accomplished by solving the following:

$$\left.\begin{aligned} v &= \frac{U_1}{U_2}\Bigg|_j^{n+1} \\ u &= \frac{U_2 + \sqrt{U_2^2 - 4U_1^2k(1-k)(1-v^2)}}{2U_1(1-k)}\Bigg|_j^{n+1} \\ \rho &= \frac{U_1}{\zeta u_1}\Bigg|_j^{n+1} \quad ; \quad p = \rho(1-u^2-v^2) \end{aligned}\right\} \tag{21}$$

Constructing a technique that will give a physically realistic solution of the conditions on a solid boundary is difficult in a predictor-corrector sequence since strict application requires an imaginary point inside the body. Abbett (ref. 16) developed a technique that satisfies the surface tangency

condition and relies on information provided by the finite-difference equations. For the upper and lower surfaces, respectively, the predictor equations are written as

$$\overline{U_{N_\xi}^{n+1}} = U_{N_\xi}^{n} - \left(\frac{\Delta x}{\Delta \xi}\right)\left(F_{N_\xi}^{n} - F_{N_\xi - 1}^{n}\right) \tag{22}$$

and

$$\overline{U_{1}^{n+1}} = U_{1}^{n} - \frac{\Delta x}{\Delta \xi}\left(F_{2}^{n} - F_{1}^{n}\right) \tag{23}$$

Modified corrector equations that maintain second-order accuracy at the upper and lower surfaces, respectively, are given by

$$U_{N_\xi}^{n+1} = \frac{1}{2}\left[U_{N_\xi}^{n} + \overline{U_{N_\xi}^{n+1}} - \frac{\Delta x}{\Delta \xi}\left(\overline{F_{N_\xi}^{n+1}} - \overline{F_{N_\xi - 1}^{n+1}}\right) - \frac{\Delta x}{\Delta \xi}\left(F_{N_\xi}^{n} - 2F_{N_\xi - 1}^{n} + F_{N_\xi - 2}^{n}\right)\right] \tag{24}$$

and

$$U_{1}^{n+1} = \frac{1}{2}\left[U_{1}^{n} + \overline{U_{1}^{n+1}} - \frac{\Delta x}{\Delta \xi}\left(\overline{F_{2}^{n+1}} - \overline{F_{1}^{n+1}}\right) - \frac{\Delta x}{\Delta \xi}\left(F_{3}^{n} - 2F_{2}^{n} - F_{1}^{n}\right)\right] \tag{25}$$

After the corrector equations are decoded at the boundaries, the flow variables will not necessarily satisfy the boundary conditions at the wall. The technique for satisfying the boundary conditions depends on a scheme for matching the boundary-layer solution.

The coordinates of the upper boundary are determined from

$$y_u = y_{u_o} + x \tan \delta_u \tag{26}$$

where δ_u is the deflection angle of the upper wall. When matching to the output of the boundary-layer solution, the lower boundary is specified by a table of coordinates. These coordinates are used to fit a parabola of the form

$$y = ax^2 + bx + c \tag{27}$$

between each set of three consecutive points. The three points used to determine the coefficients in the above equation were chosen so that two of the points should have $x > x^{n+1}$. The slope of the boundary is found from the derivative of equation (27).

Matching scheme—Two techniques for matching the inviscid and viscous solutions were investigated: (1) requiring tangency along the matching contour and (2) forcing the inviscid solution to agree with the u and v velocity components from the viscous solutions along the matching line. For the first matching scheme, the flow angle from the decoded corrector equations on the boundary is found from

$$\delta = \tan^{-1}\frac{v}{u} \tag{28}$$

This flow angle is compared with the slope of the boundary at x^{n+1}. If the two angles disagree, then a Prandtl-Meyer turning is applied at the new body point using

$$\frac{p}{p_j^{n+1}} = 1 - \gamma M \Delta\delta + \frac{\gamma M}{M}\left[\frac{\gamma+1}{4}(M^2) - 1\right]\Delta\delta^2 \tag{29}$$

where $\Delta\delta$ is the difference in the two angles and

$$M = M^2/\sqrt{M^2-1} \tag{30}$$

Note that the sign of $\Delta\delta$ will result in either an expansion ($\Delta\delta > 0$) or an isentropic compression ($\Delta\delta < 0$) and the pressure, resulting from equation (19), is taken as the predicted pressure on the body at data line N+1. The density is found from

$$\rho_j^{n+1} = \left[pC\right]^{1/\gamma} \tag{31}$$

where $C = e^{-S-S_r/c_v}$ and S_r is some reference entropy. Once p and ρ are known at the boundaries, the total velocity is obtained from

$$q = \sqrt{1 - (p/\rho)} \tag{32}$$

The velocity components then result from the tangency condition at the boundaries. This technique was applied on the upper boundary throughout both matching schemes investigated. With this matching scheme, two different matching boundaries were considered - δ^* and an arbitrary streamline where the Mach number remained supersonic throughout the interaction. Results are presented only for the latter case since similar results were obtained for both matching contours.

The second matching scheme forced the inviscid solution to match values of u and v given by the viscous solution along the matching contour, here taken as the boundary-layer edge. This technique does not impose the tangency condition along the matching boundary, but rather allows for mass exchange from the inviscid to viscous portions of the flow, a physically realistic situation. Since u and v along the matching contour are now taken to be known, these values are used in the decode equations (21) to solve for p^{n+1} and ρ^{n+1}.

Navier-Stokes Solutions

Solutions to the Navier-Stokes equations presented here were obtained from several sources. Solutions of MacCormack (ref. 3), MacCormack and Baldwin (ref. 11), Messina (unpublished), and Skoglund and Gay (ref. 6) were obtained from the sources cited, while additional solutions were obtained in the present study using the computer codes of MacCormack and Baldwin (ref. 11) and Carter (ref. 10).

Space does not permit a detailed description of the differences and similarities of the several codes considered. There are, however, some striking differences and similarities in the several solutions presented which warrant discussion in some detail. Figure 1 shows the envelope of four Navier-Stokes solutions obtained from references 3 and 10 to 12, together with the data of Hakkinen et al. (ref. 17), for an unseparated, laminar-boundary-layer, shock-wave interaction at M = 2. Two points immediately come to mind: first, the large discrepancy in skin friction and the relatively small discrepancy in surface pressure. At first glance, this implies a low sensitivity of the pressure distribution to the skin-friction distribution and a lack of uniqueness in the Navier-Stokes solutions. However, a sequence of solutions obtained here using MacCormack and Baldwin's (ref. 11) code, with successive mesh refinement in the outer inviscid flow, shows differences in C_f of the same order as those shown in figure 1. This arises from the fact that for the coarsest mesh considered, the externally generated shock wave takes on a thickness that, when projected onto the boundary layer, is of the same order as the length of interaction. The viscous flow is then responding to a continuous compression rather than an imposed shock wave. As the nodal structure was refined, the skin-friction distribution approached a single curve.

Figure 2 shows a similar envelope of Navier-Stokes solutions obtained from references 6, 8, 10, and 11, together with experimental data for a well-separated, laminar-boundary-layer, shock-wave interaction (ref. 17). The results here are similar to those discussed above and the same conclusions can be drawn.

The point of the foregoing presentation is not to show how poorly Navier-Stokes solutions perform but rather to induce the user of Navier-Stokes codes to examine his results critically and, in particular, to examine the computational mesh dimensions in the light of the smallest relevant physical scale in the problem under consideration.

In subsequent sections, the boundary-layer calculation scheme developed is compared to the Navier-Stokes solutions of MacCormack (ref. 3).

RESULTS

The results of the inverse boundary-layer method are compared with Navier-Stokes solutions and with experimental data. The flows considered all occur on a flat plate and the pressure rise is caused by an externally generated shock wave. The specific flow parameters and experiments considered are listed in table 1.

Table 1

Reference	M_∞	Re	p_f/p_o	Remarks
17*	2	1.84×10^5	1.2	Laminar
17*	2	1.96×10^5	1.4	Laminar
18	1.47	4×10^6/ft	2.25	Turbulent
19	2.93	5.7×10^7/m	2.5	Turbulent
19*	2.93	5.7×10^7/m	5.0	Turbulent

*Navier-Stokes solutions available.

Finally, we will describe the progress made, to date, in coupling the inverse boundary-layer method to the inviscid calculation scheme to provide a complete flow-field prediction method.

Laminar-Boundary-Layer, Shock-Wave Interaction

Two laminar-boundary-layer, shock-wave interactions are considered: an unseparated interaction at $M = 2.0$ having an overall pressure rise p_f/p_o of 1.2 and a well-separated interaction at $M = 2.0$ having an overall pressure rise p_f/p_o of 1.4. These two interactions correspond to the experiments of Hakkinen et al. (ref. 17), as shown in figures 6a and 6b, respectively, of that report. For convenience, these interactions will be called Hakkinen 6a and 6b.

Note that in this and all subsequent comparisons with Navier-Stokes solutions, the skin-friction distribution obtained from the Navier-Stokes solution was input to the inverse boundary-layer method. This procedure ensures that a comparison of other parameters, that is, velocity and pressure distributions, provides a true measure of the validity of the boundary-layer assumption, without the peripheral considerations of downstream boundary conditions or matching conditions between viscous and inviscid flow. However, some differences can arise even in this case because of the order of the difference approximation used. The present inverse method is third-order accurate in wall shear as opposed to first-order accuracy imposed by assuming a linear variation of velocity with distance away from the wall in the Navier-Stokes solutions. An examination of the differences attributable to this assumption indicates that C_f can vary ±10 percent for the same velocity profile, depending on the order of curve fit used to deduce the derivative at the wall.

Figure 3 compares the pressure distribution obtained from present methods with a refined mesh Navier-Stokes calculation using Hung and MacCormack's code (ref. 9) for Hakkinen 6a. The two solutions are nearly indistinguishable everywhere and they are in reasonable agreement with the data. In figure 4, the velocity distributions at the x location corresponding to the minimum value of C_f (fig. 3) are compared. The differences between the present method and MacCormack's solution are not large and are largely attributable to differences in transport properties, that is, $Pr = 1$ and $\mu/\mu_o = T/T_o$ in the present method and $Pr = 0.72$ and μ from the Sutherland law in MacCormack's code.

Figure 5 shows the streamwise pressure distribution for Hakkinen 6a, for $y = 0$, $\delta/2$, δ, as computed by MacCormack (ref. 3). These curves are essentially indistinguishable and hence, within the boundary layer, $\partial p/\partial y \simeq 0$. This, in turn, implies a trivial solution to the y momentum equation which, from the usual boundary order-of-magnitude arguments, indicates that the boundary-layer equations are adequate for this flow.

Figure 6 compares the pressure distribution obtained from the present method with that of MacCormack's solution for Hakkinen 6b. For this case, a slight difference in surface pressure distribution is obtained near $x/L = 0.15$.

Figure 7 compares the velocity profiles obtained from the present method and from MacCormack's method for Hakkinen 6b. Differences between the profiles are explicable in terms of differences in transport properties discussed previously. Figure 8 shows the streamwise pressure distributions for Hakkinen 6b, as computed by MacCormack (ref. 3). This figure shows the normal pressure gradient developing in about the same region noted in figure 6 ($x/L = 0.15$ corresponds to $x/\Delta x = 20$). This normal pressure gradient appears to be an inertial effect associated with strong streamline curvature in the outer portion of the boundary layer where $M(y) \rightarrow M_e$. For this case, the boundary-layer method predicts a relatively large value of $|v_e/u_e|$ (not shown), which indicates the beginning of a breakdown of the boundary-layer approximation.

Turbulent Boundary-Layer, Shock-Wave Interaction

The question of the validity of boundary-layer theory in turbulent boundary-layer, shock-wave interactions is somewhat less clear than for laminar interactions. This is true for three reasons. First, few Navier-Stokes solutions with simple turbulence models are available for comparison (ref. 18). Second, the current turbulence models are demonstrably inadequate for flows with rapidly changing boundary conditions and, third, only a few experiments are available in supersonic turbulent flow which are sufficiently detailed to permit a useful comparison. Because of these facts, only a cursory comparison of results of the present method with both Navier-Stokes solutions and experimental data can be made.

Figure 9 compares the present method with the data of Seddon (ref. 19), for a normal shock-wave, turbulent-boundary-layer interaction with an initial Mach number of 1.47. For this case, the experimentally determined value of $C_f(x)$ was input to the inverse boundary-layer method in the attached-flow regime. For the reversed-flow region, where no data were available, three estimates of C_f were made (defined by the solid, dashed, and dot-dashed lines in the upper half of figure 9). The corresponding pressure distributions are shown in the lower half of figure 9. Two conclusions can be drawn from this figure: first, the boundary-layer equations are capable of reproducing the observed behavior and, second, the pressure distribution is sufficiently sensitive to variations in C_f to permit a coupled solution to distinguish between similar distributions of skin-friction coefficient.

Figure 10 shows a comparison of a direct calculation using the present method with the data of reference 20. The experimental skin-friction distribution shown was deduced from the measured mean velocity profiles using the method of reference 21. These data were taken at a free-stream Mach number of 2.93 and a unit Reynolds number of 5.7×10^7 m^{-1}. The pressure rise was effected by a shock generator set at 7° incidence to the oncoming flow. As noted above, the predicted results were obtained for this case by calculation in the direct mode, that is, $P(x)$ was specified and C_f computed. The two predicted skin-friction distributions shown in the upper portion of figure 10 result from two

turbulence models used for this calculation. The equilibrium model is that described above while the exponential lag model is that suggested by Rose and Johnson (ref. 22) and subsequently used with some success in the Navier-Stokes calculations of reference 23 (see also ref. 18). One may conclude then that, given the appropriate turbulence model, the boundary-layer equations are adequate to describe flows of this type.

The last case considered was also taken from references 20 and 21. The initial flow properties were the same as those discussed in figure 10 but the shock generator angle was set at 13° to the oncoming flow. As shown in the upper portion of figure 11, the flow has an extensive region of separation $(x_{reatt} - x_{sep}) \simeq 4\delta$. For this case, the inverse boundary-layer method failed. The predicted pressure distribution shown in figure 11 indicated nearly twice the pressure rise observed experimentally. Direct solutions employing the experimentally observed pressure distribution failed to predict any separation. This might be attributed to three-dimensional effects in the experiment except that the Navier-Stokes solutions of Baldwin and Rose (see ref. 18), using a similar turbulence model, did a plausible job of predicting the flow. An examination of this solution shows extensive regions of significant normal pressure gradient.

Coupled Solutions

Figure 12 compares the pressure distributions resulting from the two coupling schemes for the Hakkinen 6b case with that given by the Navier-Stokes program of reference 3. Neither coupling scheme appears to be adequate when applied in a noniterative manner. The tendency of shock-capturing techniques to smear the shock wave over several grid points and to overshoot the pressure rise through the shock-wave reflection is evident. Perhaps the best overall qualitative agreement with the Navier-Stokes results is provided by the u-v coupling scheme; however, as noted earlier, the discontinuity in v that results from the boundary-layer calculations will strongly affect this scheme.

Truncated Navier-Stokes Equations

To circumvent the difficulties encountered in coupling viscous and inviscid flows, an alternative procedure was considered. Rather than solve coupled viscous and inviscid equations in an iterative mode, we proposed to solve the following system of equations:

$$\frac{\partial \rho}{\partial t} + \frac{\partial \rho u}{\partial x} + \frac{\partial \rho v}{\partial y} = 0$$

$$\frac{\partial \rho u}{\partial t} + \rho u \frac{\partial u}{\partial x} + \rho v \frac{\partial u}{\partial y} + \frac{\partial p}{\partial x} = \frac{\partial \tau_{xy}}{\partial y}$$

$$\frac{\partial \rho v}{\partial t} + \rho u \frac{\partial v}{\partial x} + \rho v \frac{\partial v}{\partial y} + \frac{\partial p}{\partial y} = 0$$

together with an equation of state and a consistent energy conservation relation. This was accomplished by simply removing the appropriate terms from the computer code of MacCormack and Baldwin (ref. 11). These equations converged everywhere within 1 percent of full Navier-Stokes solution for the Hakkinen cases 6a and 6b using the same mesh configuration (results not shown). The above method was slightly more efficient than the solution of the full Navier-Stokes equations because fewer operations need to be performed in the computer code.

One can deduce, however, that these equations can be solved and since they are parabolic in the streamwise variable, they can be solved by a forward-marching procedure. This latter fact would allow a first-order improvement in computational efficiency. Unfortunately, these conclusions were reached very late in the present study and time did not permit significant exploitation of the properties of these equations.

CONCLUDING REMARKS

We have demonstrated the validity of the boundary-layer equations applied to certain shock-wave, boundary-layer interactions. As has been suggested (e.g., ref. 2), solutions to the boundary-layer equations begin to depart significantly from those of the Navier-Stokes equations under the same conditions for which nontrivial normal pressure gradients are first observed in the Navier-Stokes solutions. Based on the physical argument that high-velocity flow, turning through a large angle, requires the action of a large force over a short distance, one may deduce that the normal pressure gradient arises primarily from the inviscid characteristics of the flow field. From this one may conclude that when some parameter involving both Mach number and turning angle, for example, $M_e|v_e/u_e|$, exceeds a critical value, boundary-layer theory will fail.

Despite the fact that boundary-layer theory can be shown to fail at high supersonic Mach numbers when extensive separations occur, it would appear that, for many technological problems, boundary-layer theory is quite satisfactory. This should be particularly true in the design of transonic airfoils and for engine inlets to be used on transonic and low supersonic flight vehicles when high angle-of-attack trajectories are not required.

Note that a typical solution presented here required about 3 min of CPU time on the IBM 360/67. Our experience indicates a factor of about 25 reduction in CPU time when the CDC 7600 is used. While the present inverse method is not yet a complete predictive method, it shows substantial promise if the coupling problems can be solved. Alternatively, if these problems defy solution, the truncated Navier-Stokes system described earlier appears to be potentially useful.

REFERENCES

1. Brown, S. N.; and Stewartson, K.: Laminar Separation, edited by W. R. Sears and M. Van Dyke, Annual Review of Fluid Mechanics, vol. 1, Annual Reviews, Inc., Palo Alto, Calif., 1969, pp. 45-72.

2. Murphy, J. D.: A Critical Evaluation of Analytic Methods for Predicting Laminar Boundary Layer, Shock Wave Interaction, NASA TN D-7044, 1971.

3. MacCormack, R. W.: Numerical Solution of the Interaction of a Shock Wave with a Laminar Boundary Layer, Proceedings of the 2nd International Conference on Numerical Methods in Fluid Dynamics, Lecture Notes in Physics, vol. 8, Springer-Verlag, 1971.

4. Klineberg, J. M.; and Steger, J. L.: The Numerical Calculation of Laminar Boundary Layer Separation, NASA TN D-7732, 1974.

5. Carter, J. E.: Solutions for Laminar Boundary Layers with Separation and Reattachment, AIAA Paper 74-583, 1974.

6. Skoglund, V. J.; and Gay, B. D.: Improved Numerical Techniques and of a Separated Interaction of an Oblique Shock Wave and a Laminar Boundary Layer, Bur. of Engin. Res. Rept. ME 41(69)S-068, Univ. of New Mexico, June 1969.

7. Staiano, E. F.: A General Numerical Procedure for Solutions of Viscous Compressible Flows with Shock Waves, Ph.D. dissertation, Univ. of New Mexico, May 1967.

8. MacCormack, R. W.: An Introduction to the Numerical Solution of the Navier-Stokes Equations, AIAA Paper 75-1, 1975.

9. Hung, C. M.; and MacCormack, R. W.: Supersonic and Hypersonic Laminar Flows Over a Two-Dimensional Compression Corner, AIAA Paper 75-2, 1975.

10. Carter, J. E.: Numerical Solutions of the Navier-Stokes Equations for the Supersonic Laminar Flow Over a Two Dimensional Compression Corner, NASA TR R-385, 1972.

11. MacCormack, R. W.; and Baldwin, B. S.: A Numerical Method for Solving the Navier-Stokes Equations with Application to Shock Boundary Layer Interactions, AIAA Paper 75-1, 1975.

12. Murphy, J. D.: Application of the Generalized Galerkin Method to the Computation of Fluid Flow, Presented at the AIAA Computational Fluid Dynamics Conference, Palm Springs, Calif., July 19-20, 1973.

13. Kendall, R. M.; and Bartlett, E. P.: Non-Similar Solutions of the Multicomponent Laminar Boundary Layer by an Integral Matrix Method, AIAA Preprint 67-218, 1967.

14. Lanczos, C.: Applied Analysis, Prentice-Hall, Englewood Cliffs, N.J., 1964.

15. Presley, L. L.; and Kutler, P.: Comparison of a Discrete-Shock Finite-Difference Technique and the Method of Characteristics for Calculating Internal Supersonic Flows, Presented at the AIAA Computational Fluid Dynamics Conference, Palm Springs, Calif., July 19-20, 1973.

16. Abbett, M. J.: Boundary Condition Calculation Procedures for Inviscid Supersonic Flow Fields, Presented at the AIAA Computational Fluid Dynamics Conference, Palm Springs, Calif., July 19-20, 1973.

17. Hakkinen, R. J.; Greber, I.; Trilling, L.; and Abarbanel, S. S.: The Interaction of an Oblique Shock Wave with a Laminar Boundary Layer. NASA MEMO 2-18-59W, 1959.

18. Baldwin, B. S.; and Rose, W. C.: Calculation of Shock-Separated Turbulent Boundary Layers. Aerodynamic Analyses Requiring Advanced Computers, Part I, NASA SP-347, 1975, pp. 401-417.

19. Seddon, J.: The Flow Produced by Interaction of a Turbulent Boundary Layer with a Normal Shock Wave of Strength Sufficient to Cause Separation, ARC R & M 3502, 1967.

20. Reda, D. C.; and Murphy, J. D.: Shock Wave Turbulent Boundary Layer Interaction in Rectangular Channels, Part II, The Influence of Side Wall Boundary Layers on Incipient Separation and Scale of the Interaction, AIAA Paper 73-234, 1973.

21. Rubesin, M. W.; Murphy, J. D.; and Rose, W. C.: Wall Shear in Strongly Retarded and Separated Turbulent Boundary Layers, AIAA J., vol. 12, no. 10, Oct. 1974, pp. 1442-1444.

22. Rose, W. C.; and Johnson, D. A.: A Study of Shock Wave Turbulent Boundary Layer Interaction Using Laser Velocimeter and Hot Wire Anemometer Techniques, AIAA Paper 74-95, 1974.

23. Shang, J. S.; and Hankey, W. L., Jr.: Numerical Solutions of the Navier-Stokes Equations for Supersonic Turbulent Flow Over a Compression Corner, AIAA Paper 75-4, 1975.

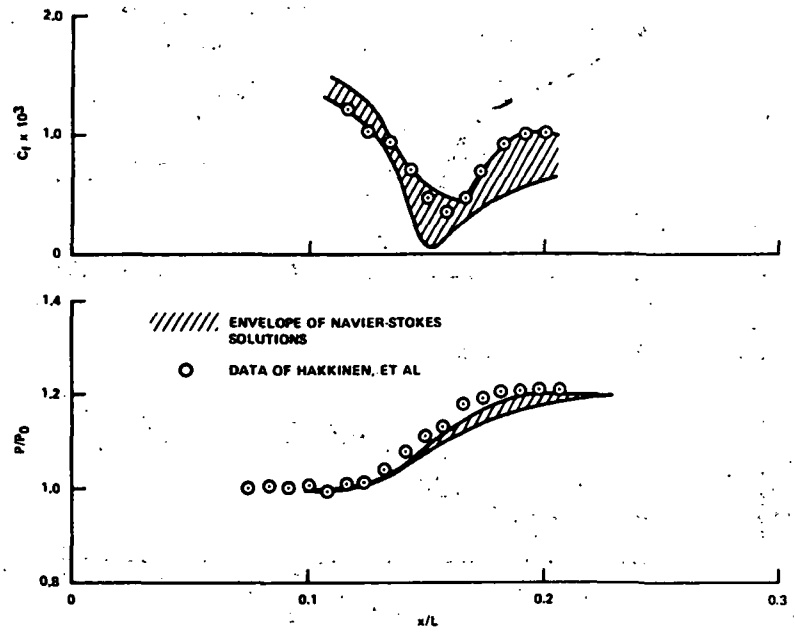

Figure 1.- Comparison of envelope of four Navier-Stokes solutions with the data of Hakkinen et al.; M = 2, $Re_{shock} = 2.84 \times 10^5$, $p_f/p_o = 1.20$.

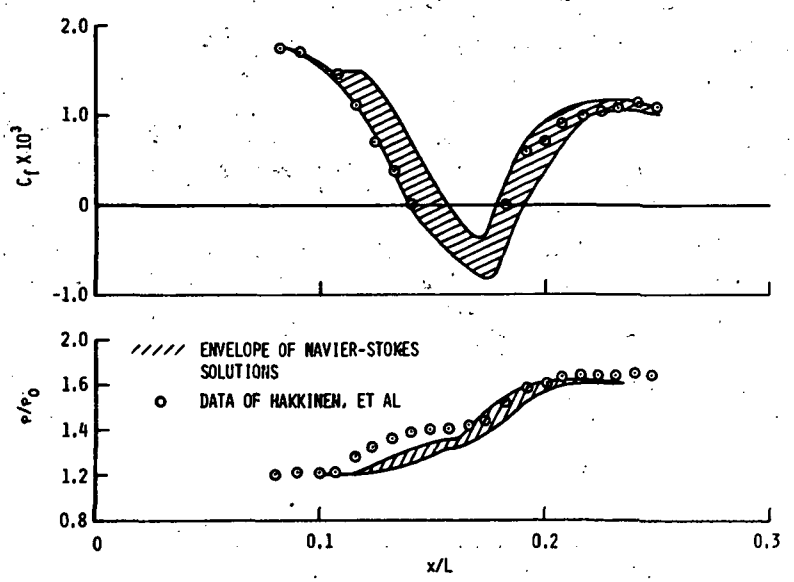

Figure 2.- Comparison of envelope of four Navier-Stokes solutions with the data of Hakkinen et al.; M = 2, $Re_{shock} = 2.96 \times 10^5$, $p_f/p_o = 1.40$.

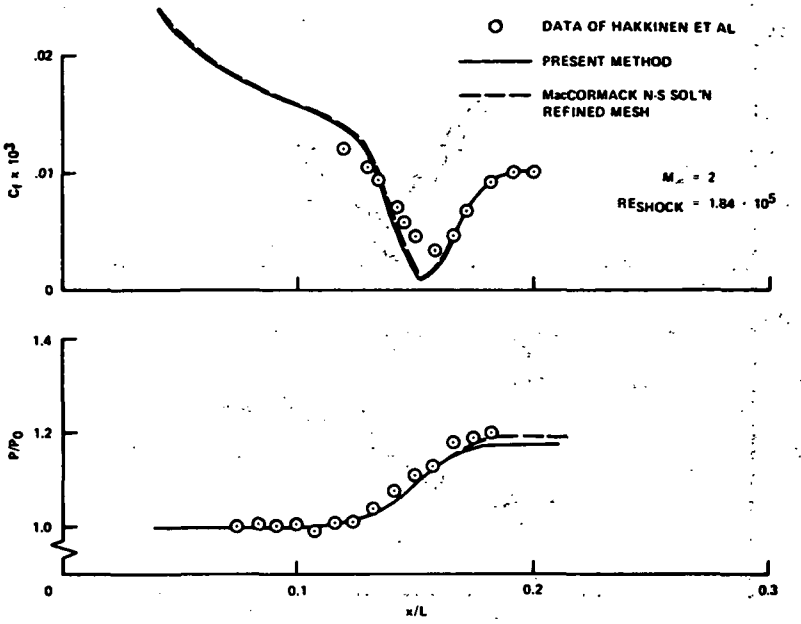

Figure 3.- Comparison of results of the present method with refined mesh calculations using Hung and MacCormack's code.

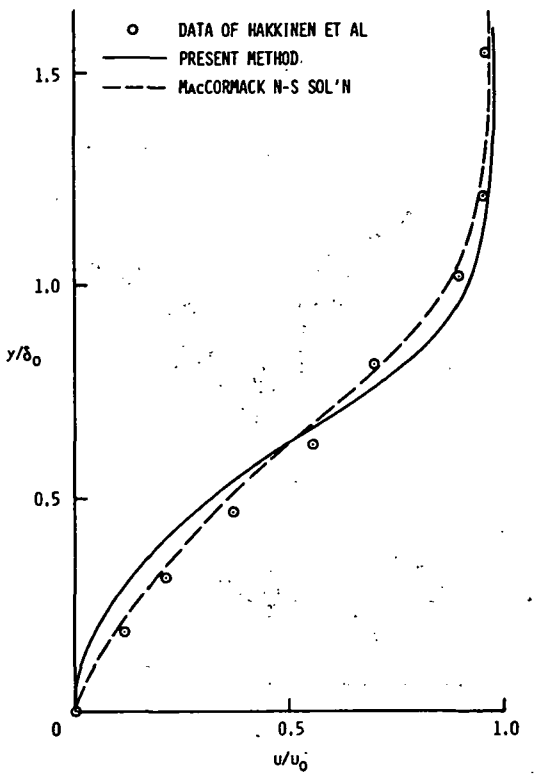

Figure 4.- Comparison of predicted velocity profiles at minimum C_f.

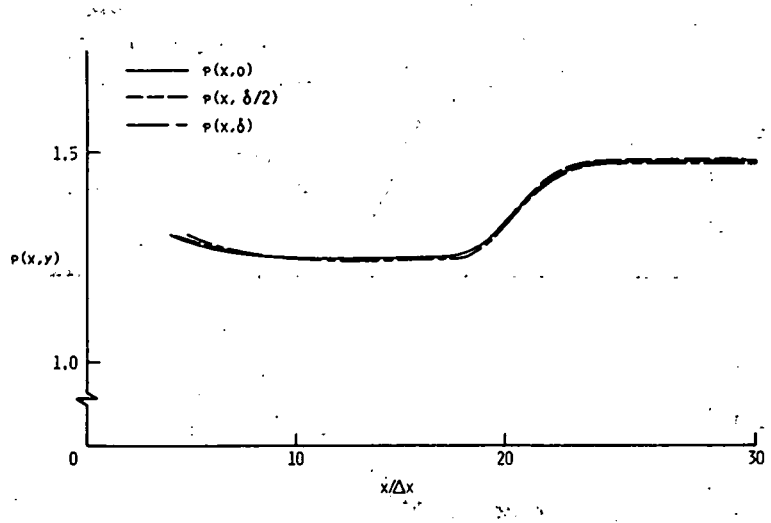

Figure 5.- Predicted pressure distributions for an unseparated laminar boundary-layer, shock-wave interaction; calculations of MacCormack.

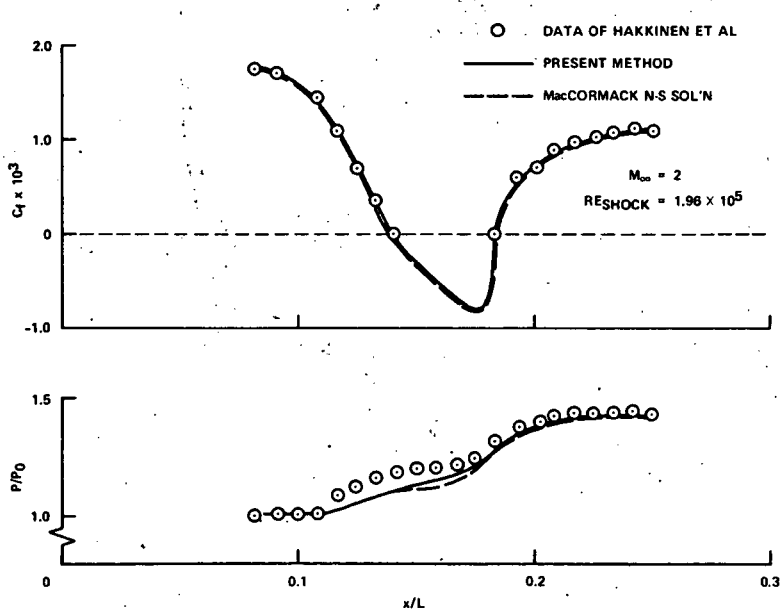

Figure 6.- Comparison of results of present method with calculations of MacCormack.

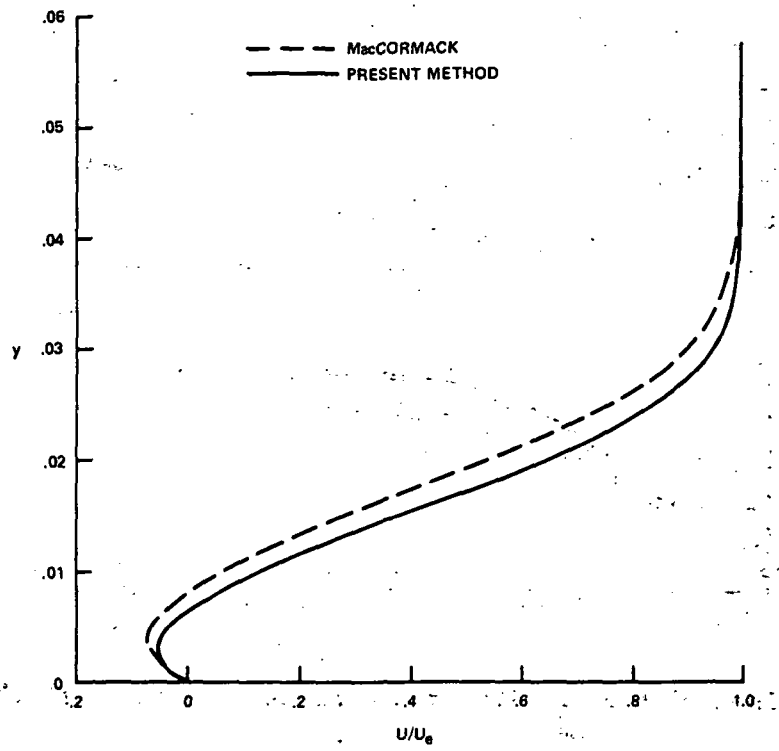

Figure 7.- Comparison of predicted velocity profiles at minimum C_f.

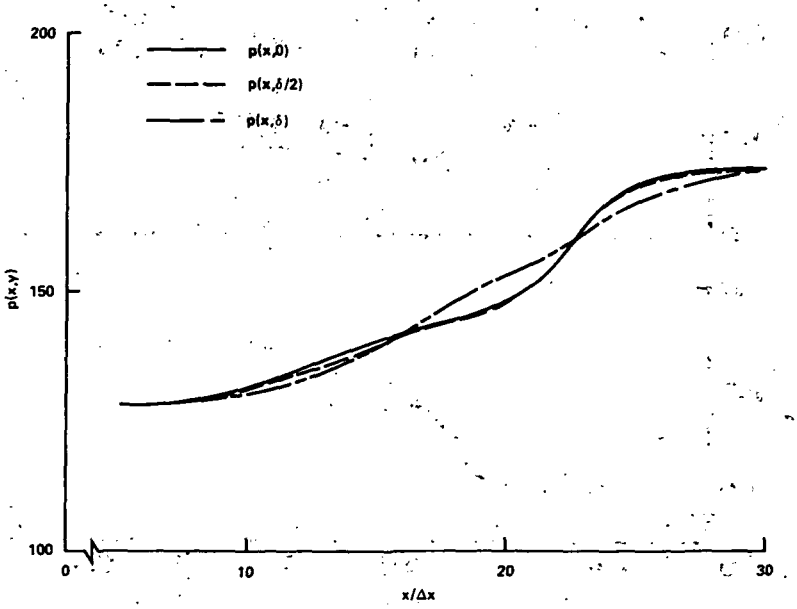

Figure 8.- Predicted pressure distributions for a separated laminar boundary-layer, shock-wave interaction; calculations of MacCormack.

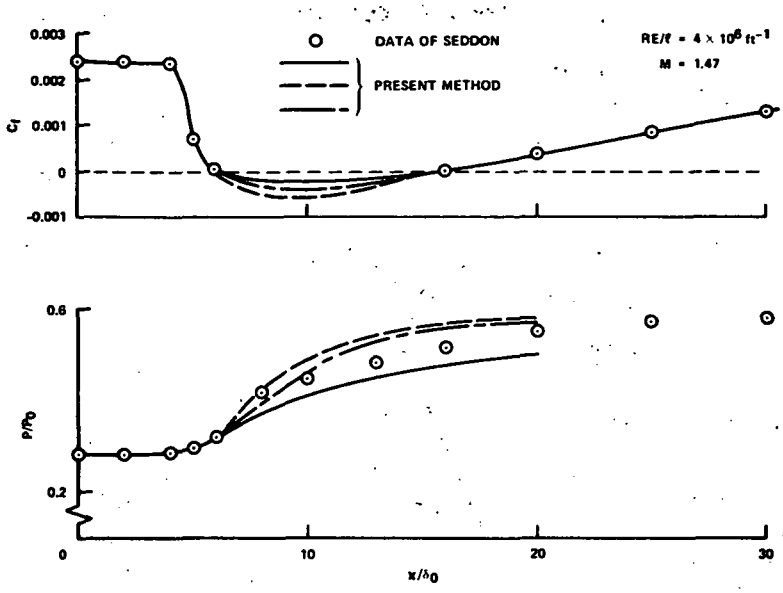

Figure 9.- Comparison of the results of the present method with the data of Seddon (ref. 18).

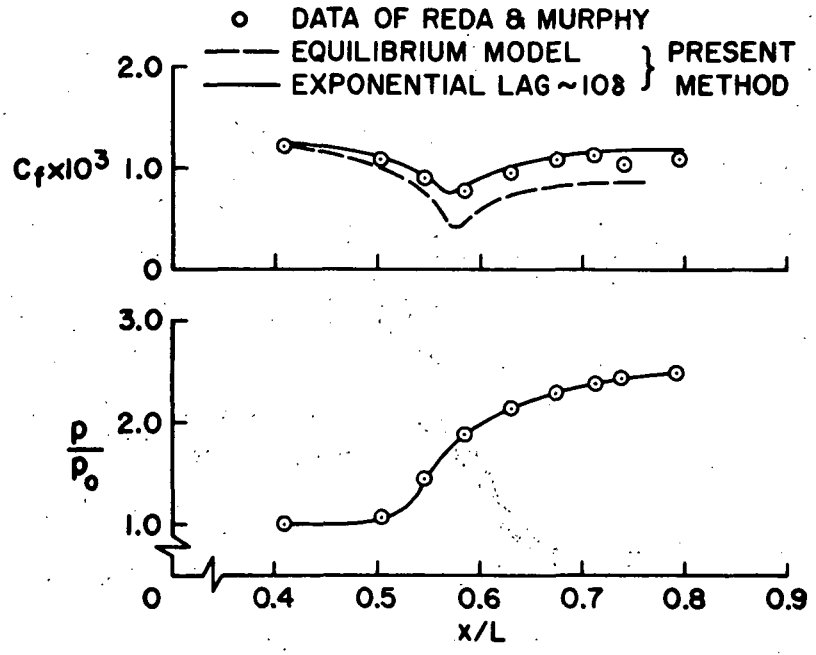

Figure 10.- Comparison of the present method with the data of reference 19; turbulent unseparated flow.

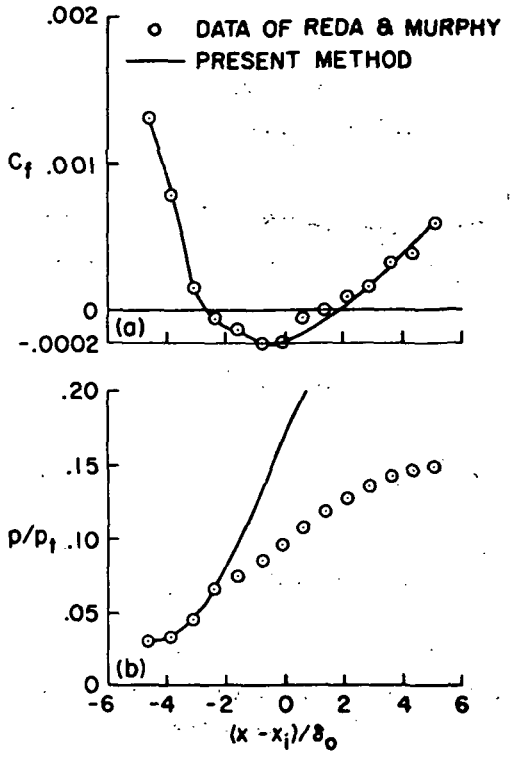

Figure 11.- Comparison of the present method with the data of reference 20; turbulent separated flow.

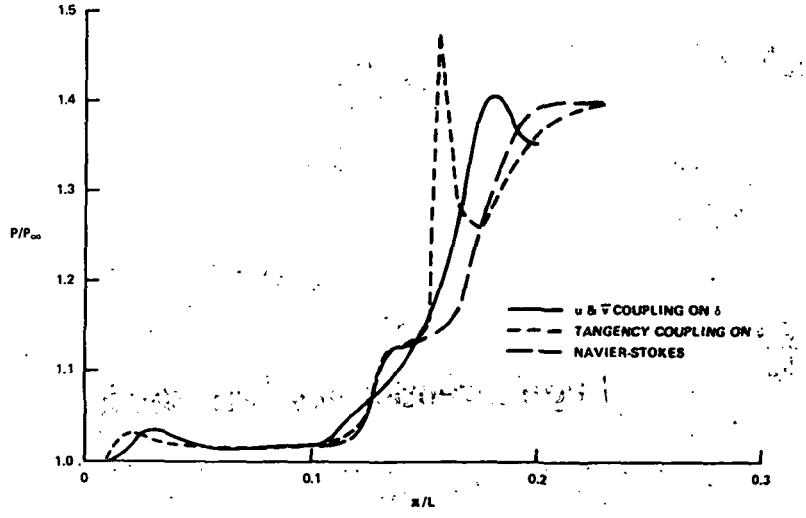

Figure 12.- Comparison of coupling schemes.